JOURNAL OF BACTERIOLOGY, Dec. 2008, p. 8137–8144 Vol. 190, No. 24
0021-9193/08/$08.00+0 doi:10.1128/JB.01049-08

Structure of L-Xylulose-5-Phosphate 3-Epimerase (UlaE) from the Anaerobic L-Ascorbate Utilization Pathway of *Escherichia coli*: Identification of a Novel Phosphate Binding Motif within a TIM Barrel Fold▽

Rong Shi,[1] Marco Pineda,[1] Eunice Ajamian,[1] Qizhi Cui,[2] Allan Matte,[2] and Miroslaw Cygler[1,2]*

Department of Biochemistry, McGill University, 3655 Promenade Sir William Osler, Montréal, Québec H3G 1Y6, Canada,[1] and Biotechnology Research Institute, NRC, 6100 Royalmount Avenue, Montréal, Québec H4P 2R2, Canada[2]

Received 28 July 2008/Accepted 21 September 2008

Three catabolic enzymes, UlaD, UlaE, and UlaF, are involved in a pathway leading to fermentation of L-ascorbate under anaerobic conditions. UlaD catalyzes a β-keto acid decarboxylation reaction to produce L-xylulose-5-phosphate, which undergoes successive epimerization reactions with UlaE (L-xylulose-5-phosphate 3-epimerase) and UlaF (L-ribulose-5-phosphate 4-epimerase), yielding D-xylulose-5-phosphate, an intermediate in the pentose phosphate pathway. We describe here crystallographic studies of UlaE from *Escherichia coli* O157:H7 that complete the structural characterization of this pathway. UlaE has a triosephosphate isomerase (TIM) barrel fold and forms dimers. The active site is located at the C-terminal ends of the parallel β-strands. The enzyme binds Zn^{2+}, which is coordinated by Glu155, Asp185, His211, and Glu251. We identified a phosphate-binding site formed by residues from the β1/α1 loop and α3′ helix in the N-terminal region. This site differs from the well-characterized phosphate-binding motif found in several TIM barrel superfamilies that is located at strands β7 and β8. The intrinsic flexibility of the active site region is reflected by two different conformations of loops forming part of the substrate-binding site. Based on computational docking of the L-xylulose 5-phosphate substrate to UlaE and structural similarities of the active site of this enzyme to the active sites of other epimerases, a metal-dependent epimerization mechanism for UlaE is proposed, and Glu155 and Glu251 are implicated as catalytic residues. Mutation and activity measurements for structurally equivalent residues in related epimerases supported this mechanistic proposal.

It has been known for nearly 70 years that various bacteria, including *Escherichia coli*, can ferment L-ascorbate (vitamin C) under anaerobic conditions (2, 10, 30, 40). This process has been demonstrated to involve proteins encoded by two divergently transcribed operons, the *ulaGR* and *ulaABCDEF* operons (3, 40, 44). The *ulaG* gene encodes L-ascorbate-6-phosphate lactonase. The *ulaABCDEF* operon encodes an L-ascorbate phosphotransferase transport system (UlaABC, formerly designated SgaTBA) responsible for the uptake and phosphorylation of L-ascorbate, and the *ulaDEF* genes encode three enzymes that catalyze the conversion of the phosphorylated, hydrolytic product of L-ascorbate, 3-keto-L-gulonate-6-phosphate, to D-xylulose-5-phosphate, which is subsequently metabolized by the pentose phosphate pathway. UlaD (formerly SgaH) decarboxylates 3-keto-L-gulonate-6-phosphate, yielding L-xylulose-5-phosphate, which is subsequently epimerized by UlaE (formerly SgaU) at C-3 to L-ribulose-5-phosphate and then epimerized by UlaF (formerly SgaE) at C-4 to D-xylulose-5-phosphate (Fig. 1) (40). Considering that *E. coli* and several other enteric bacteria are normal inhabitants of the anaerobic environment in the mammalian intestine and that L-ascorbate is a common constituent of many plant and animal tissues, it has been suggested that intestinal bacteria may compete with the intestinal mucosal cells for available sources of vitamin C (44). Recently, the metabolic system involved in the aerobic dissimilation of L-ascorbate in *E. coli* has also been investigated and has been found to be comprised of three proteins paralogous to UlaD, UlaE, and UlaF, which have been identified as YiaQ, YiaR, and YiaS, respectively (4).

For the three catabolic enzymes encoded by *ulaDEF* (UlaD, UlaE, and UlaF), only the crystal structure of UlaD has been determined previously (39). UlaD is a dimer of triosephosphate isomerase (TIM) barrels with the active site located at the dimer interface. Carboxylate side chains located at the ends of β1, β2, and β3 function as ligands for Mg^{2+}, a metal essential for activity (39). Although UlaF has not been structurally characterized, the crystal structure and biochemical characteristics of a homologous protein having 76% sequence identity, AraD, are available (22, 31). AraD is a tetramer, and each subunit is comprised of a central β-sheet flanked on either side by layers of α-helices. The activity of AraD is also metal (Zn^{2+}) dependent, and its active site is located between adjacent subunits.

Here we describe the crystal structure of UlaE, an L-xylulose-5-phosphate 3-epimerase in the ascorbate utilization pathway, and our results finalize the structural view of the three successive catabolic enzymes in this pathway. Like UlaD, UlaE has a TIM barrel fold with the active site located at the C-terminal ends of the parallel β-strands. UlaE is a dimer both in solution and in crystals, and it has a dimerization interface that differs from that of its closest structural neighbors. Soaking in $ZnCl_2$ showed that the Zn^{2+} ion binds in the active site of the

* Corresponding author. Mailing address: Biotechnology Research Institute, NRC, 6100 Royalmount Avenue, Montréal, Québec H4P 2R2, Canada. Phone: (514) 496-6321. Fax: (514) 496-5143. E-mail: mirek@bri.nrc.ca.

▽ Published ahead of print on 10 October 2008.

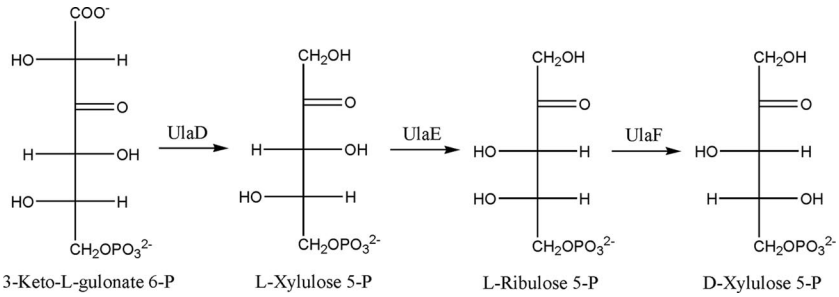

FIG. 1. Pathway for the utilization of L-ascorbate involving the catabolic enzymes UlaD, UlaE, and UlaF, which catalyze the conversion of the phosphorylated, hydrolytic product of L-ascorbate, 3-keto-L-gulonate-6-phosphate, to D-xylulose-5-phosphate. The latter compound is subsequently metabolized by the pentose phosphate pathway.

enzyme. We also observed a bound SO_4^{2-} ion. Surprisingly, this ion binds at a site different from the conserved phosphate-binding motif observed for other TIM barrel proteins. Moreover, comparison of the UlaE structure determined by using two different crystal forms revealed conformational differences in several loops encompassing the substrate-binding site, indicating that substrate-binding site flexibility is an important feature of this enzyme. Computational molecular docking performed with the assumption that the substrate phosphate binds at the observed SO_4^{2-} site and similarities of the UlaE active site structure with the active site structures of other enzymes allowed us to propose a mechanism for substrate epimerization and identify likely catalytic residues.

MATERIALS AND METHODS

Cloning, expression, and purification. The *ulaE* gene (NCBI gi 12519188) from *E. coli* O157:H7 strain EDL933 (27) was cloned into a modified pET15b vector (Novagen), yielding a fusion protein with an N-terminal His_6 tag, and was expressed in *E. coli* BL21(DE3) or the methionine auxotroph DL41(DE3) (SeMet-labeled protein) (14). One liter of terrific broth (or LeMaster medium) containing 50 μg/ml ampicillin was inoculated using an overnight culture, grown at 37°C until the absorbance at 600 nm was 0.6, induced with 100 μM isopropyl-1-thio-β-D-galactopyranoside (IPTG), and incubated for 16 h at 16°C. Cells were harvested by centrifugation (4,000 × *g*, 4°C, 25 min) and stored at −20°C. The cell pellet was resuspended in 40 ml of lysis buffer (50 mM Tris [pH 8.0], 0.4 M NaCl, 5% [vol/vol] glycerol, 0.5% [vol/vol] Triton X-100, 20 mM imidazole [pH 8], 1 mM dithiothreitol [DTT]). The cells were lysed by sonication (10 12-s bursts with 20 s between bursts), the debris was removed by ultracentrifugation (100,000 × *g*, 45 min, 4°C), and the supernatant was loaded onto 1 ml (bed volume) of Ni-nitrilotriacetic acid resin (Qiagen, Mississauga, Ontario, Canada) equilibrated with lysis buffer. The column was washed with 40 ml of lysis buffer and then with 40 ml of buffer A (50 mM Tris [pH 8.0], 1.0 M NaCl, 5% [vol/vol] glycerol, 20 mM imidazole [pH 8.0], 1 mM DTT) and 40 ml of buffer B (50 mM Tris [pH 8.0], 0.4 M NaCl, 5% [vol/vol] glycerol, 40 mM imidazole, 1 mM DTT). UlaE was eluted in buffer B containing 250 mM imidazole (pH 8.0). The eluted protein was exchanged into a buffer (20 mM Tris [pH 8.0], 20 mM NaCl, 5% [vol/vol]) glycerol, 50 mM imidazole, 5 mM DTT) for subsequent purification by anion-exchange chromatography using a PorosQ column. Dynamic light scattering measurements were obtained at room temperature using a DynaPro plate reader (Wyatt Technologies, Santa Barbara CA). Molecular mass was estimated by size exclusion chromatography using a Superdex-200 column calibrated with molecular mass standards (Sigma). SeMet-labeled protein was obtained by using the same protocol.

Crystallization. The initial crystallization conditions were determined by using hanging drop vapor diffusion at 21°C and screens prepared in house and obtained from Hampton Research (Aliso Viejo, CA). SeMet-labeled UlaE was concentrated to 12 mg/ml in buffer containing 20 mM Tris (pH 8.0), 200 mM NaCl, 5% (vol/vol) glycerol, and 5 mM DTT. The crystals were grown by equilibration of 1 μl of protein mixed with 1 μl of reservoir solution [0.6 M $(NH_4)_2SO_4$, unbuffered] over 1 ml of reservoir solution and belonged to space group $P4_32_12$ with $a = 110.4$ Å and $c = 103.0$ Å (form A) and with two molecules in the asymmetric unit and a V_m of 2.36 Å^3 Da^{-1}. Native UlaE was concentrated to 12 mg/ml in 20 mM Tris (pH 8.0)–20 mM NaCl–50 mM imidazole (pH 8.0)–5% (vol/vol) glycerol–5 mM DTT. The best crystals were obtained by equilibration of the protein with a reservoir solution containing 20% (wt/vol) polyethylene glycol 8000, 100 mM Tris (pH 8.5), 150 mM Li_2SO_4, and 50 mM arginine (condition 1) or with a reservoir solution containing 18% (wt/vol) polyethylene glycol 4000, 100 mM bis-Tris-propane (pH 7.0), and 0.5 M NaCl (condition 2). In both cases the same crystal form was obtained, space group $C222_1$ with $a = 105.0$ Å, $b = 132.6$ Å, and $c = 82.1$ Å (form B) with two molecules in the asymmetric unit with a V_m of 2.15 Å^3 Da^{-1}. Soaking native crystals from condition 1 for 2 h in reservoir solution with 2 mM $ZnCl_2$ resulted in a UlaE-SO_4^{2-}-Zn^{2+} complex, while similar soaking using the reservoir solution from condition 2 supplemented with 2 mM $ZnCl_2$ yielded a UlaE-Zn^2 complex. The cryoprotectant solution consisted of 3.0 M $(NH_4)_2SO_4$ supplemented with 15% (vol/vol) glycerol for SeMet-labeled crystals and reservoir solution supplemented with 15% (vol/vol) ethylene glycol for native crystals.

X-ray data collection, structure solution, and refinement. Diffraction data for a SeMet-labeled UlaE crystal flash cooled in a nitrogen stream at 100 K (Oxford Cryosystems, Oxford, United Kingdom) were collected to 2.7-Å resolution with a Quantum-4 charge-coupled device detector (Area Detector Systems Corp., San Diego, CA) at beamline X8C at the National Synchrotron Light Source at Brookhaven National Laboratory. Data integration and scaling were performed with HKL2000 (26). Initial phases were determined by single-wavelength anomalous dispersion at the Se peak energy. Sixteen of the 22 expected Se atoms in the asymmetric unit were located with the program SOLVE (33), and the phases were improved with the program RESOLVE (32). An initial model was built automatically by RESOLVE and was improved by ARP/wARP (28) using a data set to 2.08-Å resolution collected at beamline X29 at the National Synchrotron Light Source at Brookhaven National Laboratory. The model was completed manually using the program COOT (9) and was refined with the program REFMAC5 (23). All measured reflections were used in the refinement. The translation-libration-screw model for anisotropic temperature factors was applied (37, 38), and the refinement converged to an R_{work} value of 0.212 and an R_{free} value of 0.242. In form A the N-terminal His tag and residues 1 to 4, 158 to 174, 192 to 195, and 282 to 284 were not visible in the electron density maps.

Data sets for form B crystals were collected at the 31-ID beamline of the SGX Collaborative Access Team at Argonne National Laboratory using an MAR 165 charge-coupled device detector. One data set was obtained for crystals grown from a solution containing 150 mM Li_2SO_4, and a second data set was obtained for a crystal soaked in 2 mM $ZnCl_2$ for 2 h. An additional data set was collected near the Zn absorption edge (1.282 Å) for a crystal obtained in the absence of sulfate ions and soaked in 2 mM $ZnCl_2$ for 2 h. Attempts to obtain a UlaE–Zn^{2+}–L-ribulose-5-phosphate complex by soaking crystals in the presence of 10 to 25 mM substrate were unsuccessful. The form B crystals were solved with the program MOLREP (34) using the form A model. The form B model is more complete and contains residues 5 to 281 inclusive. Water molecules, sulfate, and Zn^{2+} ions were added to the model, which was followed by translation-libration-screw refinement. Both UlaE form A and form B models have good stereochemistry (Table 1), as analyzed with PROCHECK (20).

Molecular docking of the L-xylulose-5-phosphate substrate. Coordinates of L-Xylulose-5-phosphate were obtained from a complex of this molecule with 3-keto-L-gulonate 6-phosphate decarboxylase (PDB code 1Q6R) (39) and then minimizing with Sybyl 7.0 (Tripos, Inc., St. Louis, MO). The target protein for docking was prepared from the crystal structure of native UlaE by adding the

TABLE 1. X-ray data collection and refinement statistics

Data set	SeMet UlaE single-wavelength anomalous dispersion	SeMet UlaE-SO_4^{2-}	UlaE-SO_4^{2-}	UlaE-Zn^{2+}	UlaE-SO_4^{2-}-Zn^{2+}
Data collection					
Space group	$P4_32_12$ (form A)	$P4_32_12$ (form A)	$C222_1$ (form B)	$C222_1$ (form B)	$C222_1$ (form B)
a (Å)	110.8	110.4	102.5	104.2	105.0
b (Å)	110.8	110.4	132.5	132.6	132.6
c (Å)	103.4	103.0	82.2	81.8	82.1
Wavelength (Å)	0.9796	1.10	0.9798	1.282	0.9798
Resolution (Å)	50–2.70 (2.80–2.70)	50–2.08 (2.15–2.08)	50–2.10 (2.18–2.10)	50–2.05 (2.12–2.05)	50–2.32 (2.40–2.32)
Observed *hkl*	167,240	293,869	226,683	451,694	305,399
Unique *hkl*	33,828[c]	38,726	31,993	67,609[c]	23,425
Redundancy	4.9	7.6	7.1	6.7	13.1
Completeness (%)	100 (100)	99.8 (99.9)	96.7 (83.1)	97.6 (81.7)	94.0 (72.5)
R_{sym}[a]	0.114 (0.510)	0.074 (0.527)	0.069 (0.407)	0.072 (0.387)	0.081 (0.366)
I/σ (I)	6.7 (3.1)	12.9 (2.9)	11.4 (2.7)	12.7 (2.6)	10.7 (3.0)
Wilson B ($Å^2$)		35.5	29.9	30.1	36.4
Refinement					
R_{work} (no. of *hkl*)[b]		0.212 (36,726)	0.185 (30,355)	0.183 (33,764)	0.187 (22,235)
R_{free} (no. of *hkl*)		0.242 (1,939)	0.223 (1,620)	0.213 (1,779)	0.211 (1,151)
B-factors (no. of atoms)					
Protein		34.6 (4,041)	28.2 (4,389)	31.9 (4,387)	33.1 (4,384)
Solvent		40.9 (169)	33.1 (186)	38.5 (193)	30.1 (82)
Ligands (others)		63.1 (25)	62.0 (20)	47.0 (4)	83.2(14)
Ramachandran					
Allowed (%)		99.3	99.5	99.6	99.4
Generous (%)		0.7	0.5	0.4	0.2
Disallowed (%)		0	0	0	0.4
Root mean square deviation of bonds (Å)		0.012	0.010	0.010	0.012
Root mean square deviation of angles (°)		1.28	1.19	1.16	1.33
PDB code		3CQH	3CQI	3CQJ	3CQK

[a] $R_{sym} = (\Sigma I_{obs} - I_{avg})/\Sigma I_{avg}$.
[b] $R_{work} = (\Sigma F_{obs} - F_{calc})/\Sigma F_{obs}$.
[c] Friedel pairs were not merged in the data set.

missing side chains and hydrogen atoms. The docking program FlexX in the Sybyl 7.0 suite was used to generate and rank initial potential binding poses of L-xylulose-5-phosphate to the protein target. Based on predicted involvement of the Zn^{2+} ion in the catalytic mechanism, we selected for further energy minimization and binding free energy calculations the pose which had closest O-2 and O-3 contacts with this ion and whose phosphate group was positioned closest to that of SO_4^{2-} in the crystal structure. The protein-ligand complex was minimized using Sybyl with six distance restraints (2.1 Å and 200 kcal/mol/$Å^2$) between Zn^{2+} and O-E2 of Glu155, O-D2 of Asp185, N-D1 of His211, O-E1 of Glu251, and O-2 and O-3 of L-xylulose-5-phosphate. The AMBER ff03 force field (8, 21) was used for the protein. The binding free energy was calculated using our solvated interaction energy function (25).

Protein data bank accession codes. Coordinates for form A crystals of SeMet-UlaE and form B of the UlaE-SO_4^{2-} complex, the UlaE-Zn^{2+} complex, and the UlaE-SO_4^{2-}-Zn^{2+} complex have been deposited in the RCSB Protein Data Bank under accession codes 3CQH, 3CQI, 3CQJ, and 3CQK, respectively.

RESULTS AND DISCUSSION

Overall structure and relationship to other protein structures. The UlaE molecule adopts the TIM barrel fold (Fig. 2a). This is the most common enzyme fold among proteins in the Protein Data Bank (12, 36). Each TIM barrel consists of eight βα fold repeat units, with the eight parallel β-strands located in the interior and the eight α-helices on the exterior of the barrel. Despite the great diversity in the reactions catalyzed by TIM barrel enzymes, the active site is always at the C-terminal end of the β-strands, and the active sites are formed by residues from loops following the β-strands (βα loops). Many of the substrates or cofactors of TIM barrel enzymes contain a phosphate moiety, and, with few exceptions, the phosphate is bound by residues in strands β7 and β8 in the C-terminal half of the protein (24).

Based on the location of the Zn^{2+} and SO_4^{2-} ions, the substrate-binding site is, as expected, located at the C-terminal ends of the β-strands. The UlaE TIM barrel fold differs from a canonical TIM barrel fold in that three additional short helices (α2′, α3′, and α6′) are present within the βα loops, each following a β-strand (β2, β3, and β6, respectively).

We crystallized UlaE in two different packing environments. For the most part, in both crystal forms the molecules within the asymmetric unit had very similar structures, and the root mean square deviation was less than 0.4 Å for any pairwise comparison. There were, however, significant local conformational differences between the molecules in the two crystal forms (see below) that were important for the proposed mechanism.

While structurally UlaE is most similar to members of the xylose isomerase-like family, the levels of sequence identity between UlaE and these proteins are less than 15%. The most similar (DALI [15]) structures include *Bacillus subtilis* protein IolI (PDB code 1I60; Z score, 26.5) (43), D-xylose isomerase from *Streptomyces rubiginosus* (PDB code 4XIS; Z score, 25.5) (35), D-psicose 3-epimerase from *Agrobacterium tumefaciens*

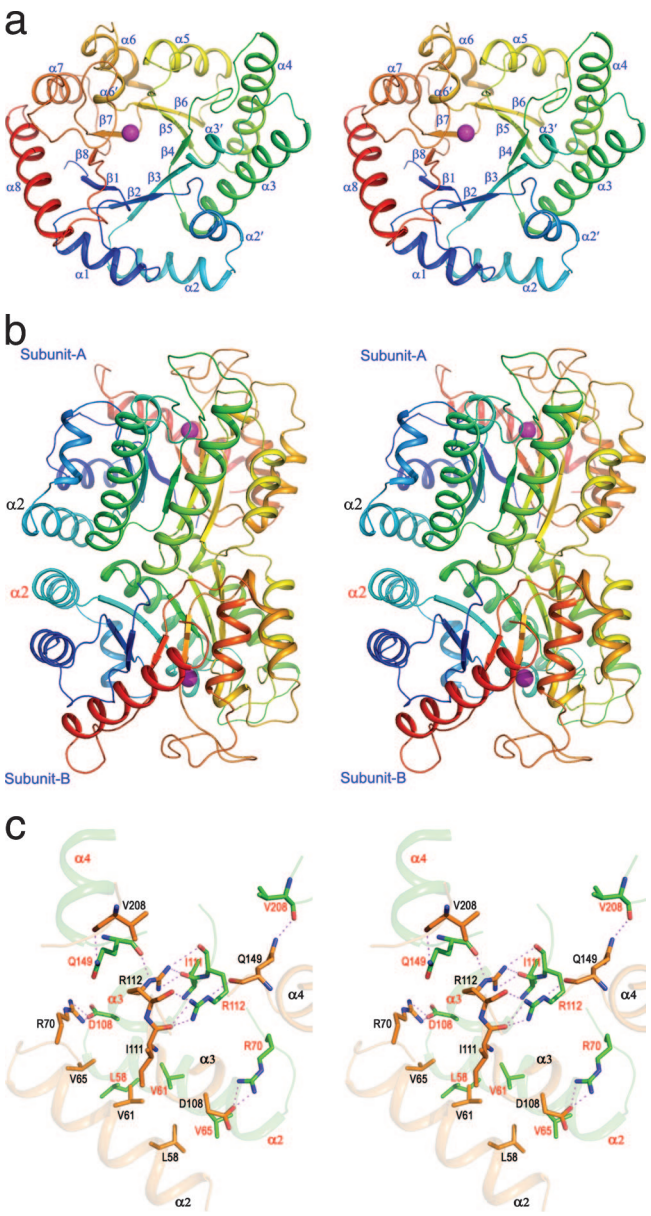

FIG. 2. Crystal structure of UlaE. (a) Cartoon representation of the UlaE monomer. The molecule is blue at the N terminus and red at the C terminus. The Zn^{2+} ion is indicated by a magenta sphere. (b) Dimer of UlaE. The dimerization interface is formed by the ends of the barrel opposite the active site (αβ loops). (c) Close-up of the dimerization interface. Subunits A and B are orange and green. The complete side chains forming hydrogen bonds are shown. The nitrogen atoms are blue, and the oxygen atoms are red. Hydrogen bonds are indicated by magenta dashed lines. The secondary structures are semitransparent. This figure and Fig. 3 and 5 were prepared using PyMol (http://pymol.sourceforge.net/).

(PDB code 2HK1; Z score, 25.4) (18), and L-rhamnose isomerase from *Pseudomonas stutzeri* (PDB code 2HCV; Z score, 22.7) (42). The root mean square deviations between UlaE and these proteins range from 2.7 to 3.4 Å for the corresponding Cα atoms. UlaE is also structurally similar to D-ribulose-5-phosphate 3-epimerase (RPE) from potato (*Solanum tuberosum*) (PDB code 1RPX; Z score, 12.1) (19), an enzyme that catalyzes the interconversion of D-ribulose 5-phosphate and D-xylulose-5-phosphate in both the reductive and oxidative pentose phosphate pathways (1). RPE belongs to a TIM barrel family that is distinct from the family containing UlaE.

Dimer structure. Despite different crystal packing environments, UlaE forms identical dimers in both crystal forms (Fig. 2b). Dimerization also occurs in solution, as indicated by size exclusion chromatography and dynamic light scattering. The two molecules form back-to-back dimers, and the interface is formed mainly by residues located within the αβ loops preceding the N-terminal ends of the β-strands and helix α2. The active sites are on opposite sides of the dimerization interface, are accessible to the solvent, and are separated by ~40 Å. Of all the αβ loops, only the α1/β2 loop is not involved in the dimer interface. Dimerization buries approximately 1,680 $Å^2$ of each subunit (as calculated with the AREAIMOL CCP4 program suite [7]), accounting for ~14% of the monomer surface area, and involves numerous van der Waals contacts and direct or water-mediated hydrogen bonds (Fig. 2c). In particular, residues Arg70, Asp108, Ile111, Arg112, Gln149, and Val208 of each subunit participate in hydrogen bonds (e.g., a salt bridge between Arg70 and Asp108′). The dimerization mode of UlaE is different from that observed for the most structurally similar proteins in the xylose isomerase-like superfamily. In the latter proteins, all three isomerases (epimerases) exist as tetramers, and the intersubunit contact regions are different from that of UlaE.

Sulfate- and Zn^{2+}-binding sites. In both crystal forms we identified a sulfate ion bound to UlaE in the same location. This is the most likely binding site for the phosphate group of the substrate. The SO_4^{2-} ion binds in a pocket near the C-terminal ends of the β-strands and is within hydrogen bonding distance of the side chains of Tyr11, Lys13, Ser77, Arg80, and Trp253 (Fig. 3a). Both Tyr11 and Lys13 are situated in the β1/α1 loop, whereas Ser77 and Arg80 are located in the short α3′ helix that follows strand β3. Of these five residues, only Trp253 is in the C-terminal region of UlaE.

The observed location of the PO_4^{3-} (SO_4^{2-}) ion-binding site differs from the locations previously observed in TIM barrel enzymes. Nagano and coworkers analyzed the phosphate-binding sites of TIM barrel fold enzymes (24) and found that the phosphate-binding sites are located in the C-terminal segments, predominantly in the β7/β8 segment and less frequently in the β5/β6 segment. A significant feature of the phosphate-binding motif is that the interaction with the phosphate moiety occurs mainly through the backbone amide groups. Although the corresponding residues are not well conserved, glycine is widely used. In UlaE, no glycine residues are present in β7 and β8, implying that the conserved phosphate-binding motif found in other TIM barrel proteins is absent in UlaE. Thus, the phosphate-binding site identified in UlaE is comprised of residues from two structural elements, β1 and α3′, in the N-terminal region. This location of the phosphate-binding site and interactions of the ion through side chains rather than through the backbone amide groups identify this binding site as a novel feature of the TIM barrel fold.

Almost all structurally related proteins contain a divalent metal-binding site (a binding site for Zn^{2+}, Mn^{2+}, Mg^{2+}, or Co^{2+}). Although the residues coordinating the metal ions are located in similar regions in these proteins, they are not structurally conserved. A cation-binding site in the UlaE active site

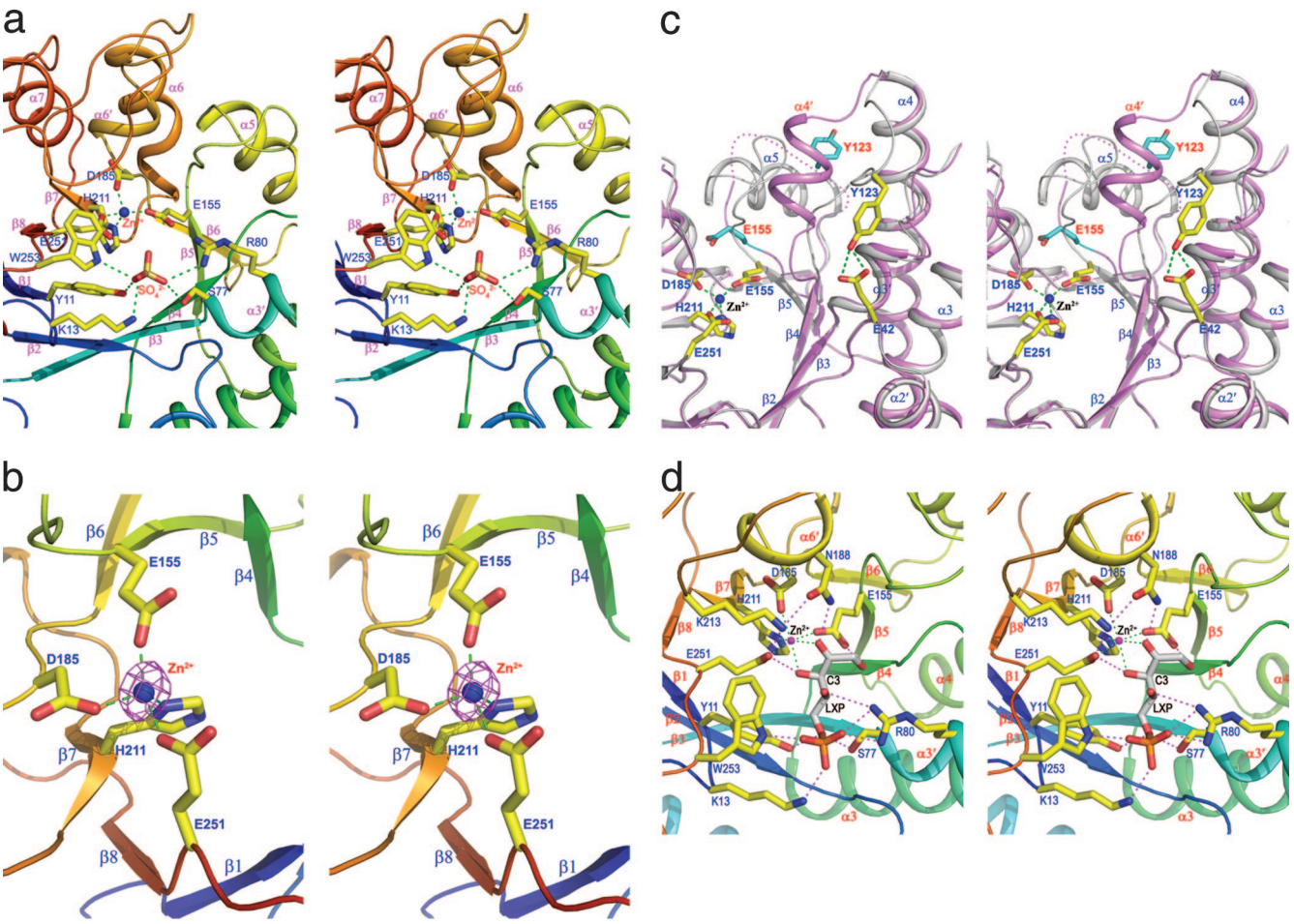

FIG. 3. Active site of UlaE. (a) UlaE-Zn^{2+}-SO_4^{2-} complex, showing the binding sites of the sulfate and zinc ions. The SO_4^{2-} ion is stabilized by Tyr11, Lys13, Ser77, Arg80, and Trp253, and the Zn^{2+} ion is coordinated by Glu155, Asp185, His211, and Glu251. The interactions are indicated by dashed lines. The colors used for the secondary structures are described in the legend to Fig. 2. (b) Anomalous map calculated using a data set collected near the Zn absorption edge (1.282 Å) and contoured at 20σ displayed near the Zn^{2+} ion-binding site. Residues coordinating zinc ions are indicated. (c) Conformational differences between form A (magenta) and form B (gray) UlaE. The β4/α4 extended loop follows different paths in the two crystal forms. Part of the β5/α5 loop and helix α5 are disordered in form A. Zn^{2+}-coordinating Glu155 is displaced in form A. The shift of Tyr123 in both crystal forms is shown. (d) Docking of L-xylulose-5-phosphate (LXP) to UlaE. The zinc ion is indicated by a magenta sphere. The potential hydrogen bonds are indicated by magenta dashed lines, and the coordination to Zn^{2+} is indicated by green dashed lines.

was revealed by soaking crystals in $ZnCl_2$ and identifying the Zn^{2+} ion by a strong (~40σ) peak in an electron density map calculated from the anomalous differences (Fig. 3b). The Zn^{2+} ion is surrounded by the C-terminal ends of four β-strands (β5, β6, β7, and β8) and is coordinated by the side chains of Glu155, Asp185, His211, and Glu251 with an average distance of ~2.1Å. These side chains allow access to the Zn^{2+} ion from one side, and we found a weakly bound water molecule in this location, potentially corresponding to the position of an oxygen atom (O-2 or O-3) of the substrate. Similar coordination of the substrate oxygen was observed in D-psicose 3-epimerase (18) and in L-rhamnose isomerase (42). There are also similar metal-binding sites in the structural homologs IolI (PDB code 1I6N) (43) and endonuclease IV (16).

Conformational changes in form A and form B models. The conformations of three regions of UlaE located predominantly in three consecutive β/α loops are different in the two crystal forms (Fig. 3c). Region Asp158-Tyr174 (loop β5/α5 and helix α5) and loop Trp192-Asp195 (β6/α6) are disordered in form A but are well ordered in form B, and loop Leu116-Asn127 (β4/α4) is ordered in both forms but follows very different paths. The presence of two ordered conformations of the β4/α4 loop suggests that both conformers may exist in solution. Superposition of the two UlaE models indicated that the disorder of these loops can be attributed to a large conformational change in the β4/α4 loop. In form B, this loop (residues 116 to 127) extends with its tip toward the distal β2/α2 loop, such that Tyr123 forms a hydrogen bond with Glu42 (Fig. 3c). The Zn^{2+}-binding site is preformed in form B. In form A the β5/α5 loop has a different conformation and repositions one of the Zn^{2+} coordinating side chains, Glu155, by ~5 Å, preventing Zn^{2+} binding, consistent with the absence of a bound metal in this crystal structure. As a consequence, one conformation is compatible with metal binding, and the other is not.

Interconversion between helical and extended conformations in proteins has been observed infrequently crystallo-

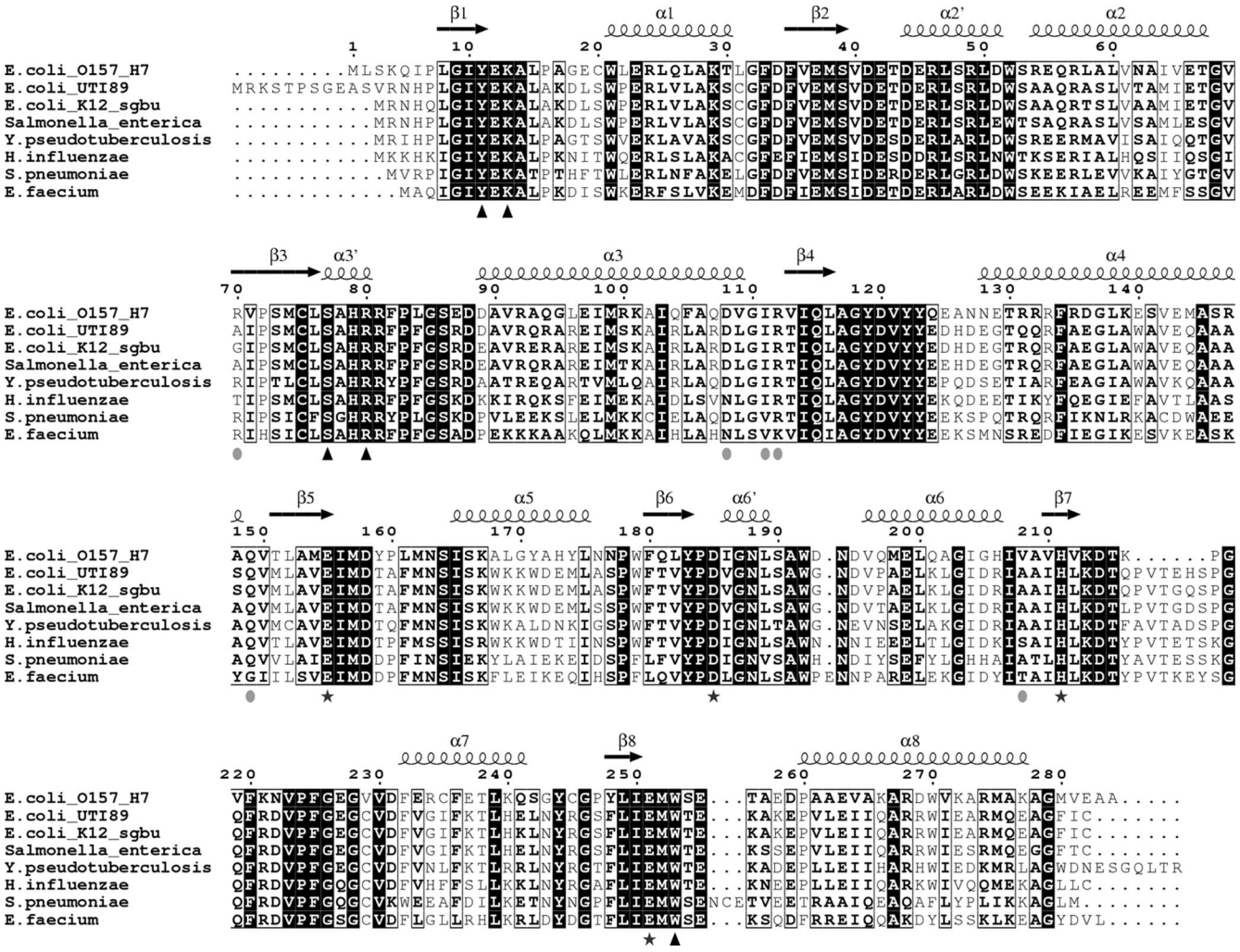

FIG. 4. Sequence alignment of *E. coli* UlaE with homologs (L-xylulose 5-phosphate 3-epimerase and hexulose-6-phosphate isomerase). The following sequences were used in this alignment: *E. coli* O157:H7 (gi 15804786), *Streptococcus pneumoniae* (gi 148985971), *Enterococcus faecium* (gi 69247869), *Yersinia pseudotuberculosis* (gi 153947045), *Salmonella enterica* (gi 56415568), *E. coli* UTI89 (gi 91213099), *Haemophilus influenzae* (gi 145628029), and *E. coli* K-12 SgbU (gi P37679). The strictly conserved residues are indicated by a dark background, and the moderately conserved residues are enclosed in boxes. The secondary structures for α-helices and β-strands in *E. coli* UlaE are indicated by Greek letters and numbers. The stars indicate the residues coordinating the zinc ion. The filled triangles indicate residues binding the sulfate or phosphate moiety. The circles indicate the residues forming hydrogen bond interactions in the dimerization interface. The alignment was generated using the program ClustalW (6), and the figure was prepared by using ESPript (13).

graphically, and almost all of the available examples indicate that the winding and unwinding of a helix are biologically relevant and convert the proteins between active and inactive forms (5, 11, 17, 29).

Docking of L-xylulose-5-phosphate and proposed catalytic mechanism. In the UlaE-Zn^{2+}-sulfate structure, the distance between Zn^{2+} and the sulfate ion is ~6.5 Å, which is compatible with the size of the substrate molecule. Since we were unable to obtain crystals of the enzyme-substrate complex either by cocrystallization or by soaking crystals in 10 to 25 mM substrate, we used molecular modeling to place L-xylulose-5-phosphate in the UlaE active site (Fig. 3d). In all the substrate binding modes resulting from docking calculations, the phosphate moiety superimposes well onto the position of the sulfate anion observed in our crystal structures (Fig. 3d). In addition, the nearby residues Asn188 and Lys213 may also be involved in substrate binding.

Based on the docking results and similarities in both the active site geometry and the chemical reactions catalyzed by UlaE and D-psicose 3-epimerase (18) and RPE(1), a similar divalent metal-dependent epimerization mechanism is expected for UlaE, with Glu155 and Glu251 within the metal ion coordination sphere playing essential catalytic roles. These residues are strictly conserved in sequences of UlaE homologues (Fig. 4). Although the overall sequence identity between UlaE and D-psicose 3-epimerase is only ~16%, structurally identical residues coordinate the metal ion in D-psicose 3-epimerase (Glu150, Asp183, His209, and Glu244) and UlaE (Glu155, Asp185, His211, and Glu251) (Fig. 5). Site-directed mutagenesis confirmed that Glu150 and Glu244 are the catalytic resi-

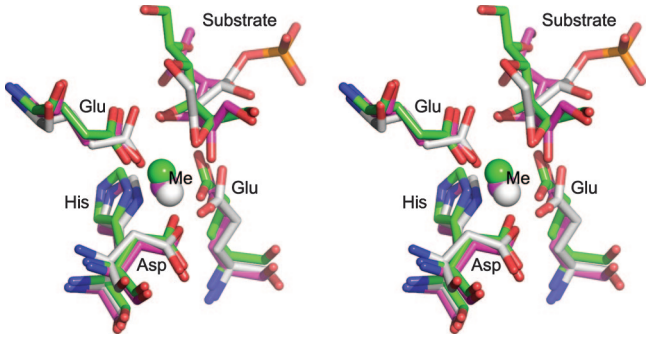

FIG. 5. Superposition of the active sites of UlaE, D-psicose 3-epimerase from *A. tumefaciens* (PDB code 2HK1), and D-tagatose 3-epimerase from *Pseudomonas cichorii* (PDB code 2QUM), showing their similarity. The modeled L-xylulose-5-phosphate substrate of UlaE, the D-fructose bound in the D-psicose 3-epimerase from *A. tumefaciens*, and the D-tagatose bound to the D-tagatose 3-epimerase from *P. cichorii* are shown. The C atoms are gray in UlaE, green in *A. tumefaciens* D-psicose 3-epimerase, and magenta in *P. cichorii* D-tagatose 3-epimerase. The metal ions are Zn^{2+} (gray) in UlaE, Mn^{2+} (green) in *A. tumefaciens* D-psicose 3-epimerase, and Mn^{2+} (magenta) in *P. cichorii* D-tagatose 3-epimerase.

dues in D-psicose 3-epimerase (18). Moreover, the same active site architecture is present in D-tagatose 3-epimerase, a homologue of D-psicose 3-epimerase, as revealed by the recently determined structure of the D-tagatose 3-epimerase complex with D-tagatose (41). Here, an Mn^{2+} ion was used rather than Zn^{2+} and was coordinated by Glu152, Asp185, His211, and Glu246, and Glu152 and Glu246 were implicated in catalysis (41). RPE also adopts a TIM barrel fold and catalyzes a Zn^{2+}-dependent epimerization reaction at C-3, similar to the reaction catalyzed by UlaE. Although the location of the active site of RPE is different from that of UlaE, RPE also contains two acidic residues, Asp36 and Asp176, in its active site that are responsible for coordinating the metal ion. The critical role of these two aspartate residues in catalysis has been confirmed by mutagenesis (1). The UlaE epimerase can also be compared with xylose isomerases, including the xylose isomerase from *S. rubiginosus* (PDB code 4XIS) (35), which exhibits high structural similarity to UlaE and utilizes a two-metal-ion (Mn^{2+}) mechanism. The first Mn^{2+} ion is coordinated by two aspartates (Asp245 and Asp287) and two glutamates (Glu181 and Glu217), and the Glu217 residue bridges to the second metal ion. Only residues coordinating the first metal are present in UlaE and in D-psicose 3-epimerase (namely, His211, Glu251, Glu155, and Asp185). The conformation of the loop that encompasses residues coordinating the second metal in xylose isomerase differs from the conformation in UlaE.

Based on the structural similarity to the other enzymes, particularly D-psicose 3-epimerase, and the presence of a bound metal ion, we postulate that in the forward reaction catalyzed by UlaE, deprotonation of C-3 of L-xylulose-5-phosphate by Glu155 generates an anionic 2,3-enediolate intermediate, which is stabilized by the metal ion (Zn^{2+}) through charge neutralization with the anionic oxygen at C-2 and by Lys213. Subsequently, reprotonation of the intermediate is achieved by Glu251, located on the side opposite Glu155, yielding the product L-ribulose-5-phosphate. The roles of these two glutamate residues are switched in the reverse reaction when L-ribulose-5-phosphate is a substrate.

ACKNOWLEDGMENTS

We thank John Wagner for performing molecular biology procedures, Ariane Proteau for determining the dimeric state of the protein in solution, and Martin Tanner for a gift of L-ribulose-5-phosphate substrate. X-ray diffraction data for this study were obtained at beamlines X8C and X29 of the National Synchrotron Light Source and by the SGX Collaborative Access Team at the Advanced Photon Source.

Financial support for the National Synchrotron Light Source comes principally from the Office of Biological and Environmental Research and Office of Basic Energy Sciences of the U.S. Department of Energy and from the National Center for Research Resources of the National Institutes of Health. Use of the Advanced Photon Source was supported by the U.S. Department of Energy Office of Science Office of Basic Energy Sciences under contract DE-AC02-06CH11357. Use of the SGX Collaborative Access Team beamline facilities at sector 31 of the Advanced Photon Source was provided by SGX Pharmaceuticals Inc., which constructed and operates the facility. This work was supported by operating grant GSP-48370 to M.C. from the Canadian Institutes of Health Research.

REFERENCES

1. **Akana, J., A. A. Fedorov, E. Fedorov, W. R. Novak, P. C. Babbitt, S. C. Almo, and J. A. Gerlt.** 2006. D-Ribulose 5-phosphate 3-epimerase: functional and structural relationships to members of the ribulose-phosphate binding (beta/alpha)8-barrel superfamily. Biochemistry **45:**2493–2503.
2. **Campos, E., J. Aguilar, L. Baldoma, and J. Badia.** 2002. The gene *yjfQ* encodes the repressor of the *yjfR*-X regulon (*ula*), which is involved in L-ascorbate metabolism in Escherichia coli. J. Bacteriol. **184:**6065–6068.
3. **Campos, E., L. Baldoma, J. Aguilar, and J. Badia.** 2004. Regulation of expression of the divergent *ulaG* and *ulaABCDEF* operons involved in L-ascorbate dissimilation in *Escherichia coli*. J. Bacteriol. **186:**1720–1728.
4. **Campos, E., C. Montella, F. Garces, L. Baldoma, J. Aguilar, and J. Badia.** 2007. Aerobic L-ascorbate metabolism and associated oxidative stress in Escherichia coli. Microbiology **153:**3399–3408.
5. **Chen, X., M. Tordova, G. L. Gilliland, L. Wang, Y. Li, H. Yan, and X. Ji.** 1998. Crystal structure of apo-cellular retinoic acid-binding protein type II (R111M) suggests a mechanism of ligand entry. J. Mol. Biol. **278:**641–653.
6. **Chenna, R., H. Sugawara, T. Koike, R. Lopez, T. J. Gibson, D. G. Higgins, and J. D. Thompson.** 2003. Multiple sequence alignment with the Clustal series of programs. Nucleic Acids Res. **31:**3497–3500.
7. **Collaborative Computational Project, Number 4.** 1994. The CCP4 suite: programs for protein crystallography. Acta Crystallogr. D **50:**760–763.
8. **Duan, Y., C. Wu, S. Chowdhury, M. C. Lee, G. Xiong, W. Zhang, R. Yang, P. Cieplak, R. Luo, T. Lee, J. Caldwell, J. Wang, and P. Kollman.** 2003. A point-charge force field for molecular mechanics simulations of proteins based on condensed-phase quantum mechanical calculations. J. Comput. Chem. **24:**1999–2012.
9. **Emsley, P., and K. Cowtan.** 2004. Coot: model-building tools for molecular graphics. Acta Crystallogr. D **60:**2126–2132.
10. **Esselen, W. B., and J. E. Fuller.** 1939. The oxidation of ascorbic acid as influenced by intestinal bacteria. J. Bacteriol. **37:**501–521.
11. **Ferguson, A. D., E. Hofmann, J. W. Coulton, K. Diederichs, and W. Welte.** 1998. Siderophore-mediated iron transport: crystal structure of FhuA with bound lipopolysaccharide. Science **282:**2215–2220.
12. **Gerlt, J. A., and F. M. Raushel.** 2003. Evolution of function in (beta/alpha)8-barrel enzymes. Curr. Opin. Chem. Biol. **7:**252–264.
13. **Gouet, P., E. Courcelle, D. I. Stewart, and F. Metoz.** 1999. ESPript: analysis of multiple sequence alignments in PostScript. Bioinformatics **15:**305–308.
14. **Hendrickson, W. A., J. R. Horton, and D. M. LeMaster.** 1990. Selenomethionyl proteins produced for analysis by multiwavelength anomalous diffraction (MAD): a vehicle for direct determination of three-dimensional structure. EMBO J. **9:**1665–1672.
15. **Holm, L., and C. Sander.** 1995. Dali: a network tool for protein structure comparison. Trends Biochem. Sci. **20:**478–480.
16. **Hosfield, D. J., Y. Guan, B. J. Haas, R. P. Cunningham, and J. A. Tainer.** 1999. Structure of the DNA repair enzyme endonuclease IV and its DNA complex: double-nucleotide flipping at abasic sites and three-metal-ion catalysis. Cell **98:**397–408.
17. **Houdusse, A., V. N. Kalabokis, D. Himmel, A. G. Szent-Gyorgyi, and C. Cohen.** 1999. Atomic structure of scallop myosin subfragment S1 complexed with MgADP: a novel conformation of the myosin head. Cell **97:**459–470.
18. **Kim, K., H. J. Kim, D. K. Oh, S. S. Cha, and S. Rhee.** 2006. Crystal structure of D-psicose 3-epimerase from Agrobacterium tumefaciens and its complex with true substrate D-fructose: a pivotal role of metal in catalysis, an active

site for the non-phosphorylated substrate, and its conformational changes. J. Mol. Biol. **361:**920–931.
19. **Kopp, J., S. Kopriva, K. H. Suss, and G. E. Schulz.** 1999. Structure and mechanism of the amphibolic enzyme D-ribulose-5-phosphate 3-epimerase from potato chloroplasts. J. Mol. Biol. **287:**761–771.
20. **Laskowski, R. A., M. W. MacArthur, D. S. Moss, and J. M. Thornton.** 1993. PROCHECK: a program to check the stereochemical quality of protein structures. J. Appl. Crystallogr. **26:**283–291.
21. **Lee, M. C., and Y. Duan.** 2004. Distinguish protein decoys by using a scoring function based on a new AMBER force field, short molecular dynamics simulations, and the generalized born solvent model. Proteins **55:**620–634.
22. **Luo, Y., J. Samuel, S. C. Mosimann, J. E. Lee, M. E. Tanner, and N. C. Strynadka.** 2001. The structure of L-ribulose-5-phosphate 4-epimerase: an aldolase-like platform for epimerization. Biochemistry **40:**14763–14771.
23. **Murshudov, G. N., A. A. Vagin, A. Lebedev, K. S. Wilson, and E. J. Dodson.** 1999. Efficient anisotropic refinement of macromolecular structures using FFT. Acta Crystallogr. D **55:**247–255.
24. **Nagano, N., C. A. Orengo, and J. M. Thornton.** 2002. One fold with many functions: the evolutionary relationships between TIM barrel families based on their sequences, structures and functions. J. Mol. Biol. **321:**741–765.
25. **Naim, M., S. Bhat, K. N. Rankin, S. Dennis, S. F. Chowdhury, I. Siddiqi, P. Drabik, T. Sulea, C. I. Bayly, A. Jakalian, and E. O. Purisima.** 2007. Solvated interaction energy (SIE) for scoring protein-ligand binding affinities. 1. Exploring the parameter space. J. Chem. Infect. Model. **47:**122–133.
26. **Otwinowski, Z., and W. Minor.** 1997. Processing of X-ray diffraction data collected in oscillation mode. Methods Enzymol. **276:**307–326.
27. **Perna, N. T., G. I. Plunkett, F. R. Blattner, B. Mau, and F. R. Blattner.** 2001. Genome sequence of enterohaemorrhagic *Escherichia coli* O157:H7. Nature **409:**529–533.
28. **Perrakis, A., R. Morris, and V. S. Lamzin.** 1999. Automated protein model building combined with iterative structure refinement. Nat. Struct. Biol. **6:**458–463.
29. **Polekhina, G., S. Thirup, M. Kjeldgaard, P. Nissen, C. Lippmann, and J. Nyborg.** 1996. Helix unwinding in the effector region of elongation factor EF-Tu-GDP. Structure **4:**1141–1151.
30. **Richter, H. E., J. Switala, and P. C. Loewen.** 1988. Effect of ascorbate on oxygen uptake and growth of *Escherichia coli* B. Can. J. Microbiol. **34:**822–825.
31. **Samuel, J., Y. Luo, P. M. Morgan, N. C. Strynadka, and M. E. Tanner.** 2001. Catalysis and binding in L-ribulose-5-phosphate 4-epimerase: a comparison with L-fuculose-1-phosphate aldolase. Biochemistry **40:**14772–14780.
32. **Terwilliger, T. C.** 2002. Automated structure solution, density modification and model building. Acta Crystallogr. D **58:**1937–1940.
33. **Terwilliger, T. C., and J. Berendzen.** 1999. Automated MAD and MIR structure solution. Acta Crystallogr. D **55:**849–861.
34. **Vagin, A., and A. Teplyakov.** 1997. MOLREP: an automated program for molecular replacement. J. Appl. Crystallogr. **30:**1022–1025.
35. **Whitlow, M., A. J. Howard, B. C. Finzel, T. L. Poulos, E. Winborne, and G. L. Gilliland.** 1991. A metal-mediated hydride shift mechanism for xylose isomerase based on the 1.6 A Streptomyces rubiginosus structures with xylitol and D-xylose. Proteins **9:**153–173.
36. **Wierenga, R. K.** 2001. The TIM-barrel fold: a versatile framework for efficient enzymes. FEBS Lett. **492:**193–198.
37. **Winn, M. D., M. N. Isupov, and G. N. Murshudov.** 2001. Use of TLS parameters to model anisotropic displacements in macromolecular refinement. Acta Crystallogr. D **57:**122–133.
38. **Winn, M. D., G. N. Murshudov, and M. Z. Papiz.** 2003. Macromolecular TLS refinement in REFMAC at moderate resolutions. Methods Enzymol. **374:**300–321.
39. **Wise, E. L., W. S. Yew, J. A. Gerlt, and I. Rayment.** 2003. Structural evidence for a 1,2-enediolate intermediate in the reaction catalyzed by 3-keto-L-gulonate 6-phosphate decarboxylase, a member of the orotidine 5′-monophosphate decarboxylase suprafamily. Biochemistry **42:**12133–12142.
40. **Yew, W. S., and J. A. Gerlt.** 2002. Utilization of L-ascorbate by *Escherichia coli* K-12: assignments of functions to products of the *yjf-sga* and *yia-sgb* operons. J. Bacteriol. **184:**302–306.
41. **Yoshida, H., M. Yamada, T. Nishitani, G. Takada, K. Izumori, and S. Kamitori.** 2007. Crystal structures of D-tagatose 3-epimerase from Pseudomonas cichorii and its complexes with D-tagatose and D-fructose. J. Mol. Biol. **374:**443–453.
42. **Yoshida, H., M. Yamada, Y. Ohyama, G. Takada, K. Izumori, and S. Kamitori.** 2007. The structures of L-rhamnose isomerase from Pseudomonas stutzeri in complexes with L-rhamnose and D-allose provide insights into broad substrate specificity. J. Mol. Biol. **365:**1505–1516.
43. **Zhang, R. G., I. Dementieva, N. Duke, F. Collart, E. Quaite-Randall, R. Alkire, L. Dieckman, N. Maltsev, O. Korolev, and A. Joachimiak.** 2002. Crystal structure of Bacillus subtilis ioli shows endonuclase IV fold with altered Zn binding. Proteins **48:**423–426.
44. **Zhang, Z., M. Aboulwafa, M. H. Smith, and M. H. Saier, Jr.** 2003. The ascorbate transporter of *Escherichia coli*. J. Bacteriol. **185:**2243–2250.